1. Ayebatonye EPEMU[1], 2. Pauline OBE[2], 3. Emeka OBE[3]

Department of Electrical/Electronic Engineering, Federal University of Petroleum Resources Effurun, Effurun, Delta State, Nigeria (1),
Department of Industrial Technical Education, University of Nigeria, Nsukka, Nigeria (2),
Department of Electrical Engineering, University of Nigeria, Nsukka, Nigeria (3)
ORCID. 1. 0000-0003-0055-214X, 2. 0000-0001-9530-2009, 3. 0000-0002-4766-2859

doi:10.15199/48.2021.10.14

Modelling and Analysis of Concentrated and Distributed Winding Synchronous Reluctance Motors in Direct-Phase Variables and Finite Element Analysis

Abstract. *The modelling and analysis of a proposed line-start three-phase concentrated (overlapping) and conventional distributed winding synchronous reluctance motors was carried out in this study. The machine inductances were determined using Winding Function Theory (WFT) and the analysis of the machine was done in Direct-Phase Variables (DPV). The machine performance characteristics such as Speed, Torque and Phase currents were observed. ANSYS Finite Element Analysis (FEA) software was used to validate and show the viability of the models as harmonics are taken into account in the FEA simulation. The results obtained from the FEA simulation showed the presence of MMF harmonics and airgap permeance harmonics that produced torque ripples. Although distributed winding SynRM showed slightly better overload capability the proposed concentrated winding SynRM will be easier to construct due to its fewer stator slots.*

Streszczenie. *W pracy przeprowadzono modelowanie i analizę zaproponowanych synchronicznych silników reluktancyjnych trójfazowych skoncentrowanych (nakładających się) i konwencjonalnych o uzwojeniu rozproszonym. Indukcyjność maszyny wyznaczono za pomocą teorii funkcji uzwojenia (WFT), a analizę maszyny przeprowadzono w zmiennych fazach bezpośrednich (DPV). Zaobserwowano charakterystyki pracy maszyny, takie jak prędkość, moment obrotowy i prądy fazowe. Oprogramowanie ANSYS do analizy elementów skończonych (FEA) zostało użyte do walidacji i wykazania wykonalności modeli, ponieważ w symulacji MES uwzględniane są harmoniczne. Wyniki uzyskane z symulacji FEA wykazały obecność harmonicznych MMF i harmonicznych przepuszczalności szczeliny powietrznej, które powodowały tętnienia momentu obrotowego. Chociaż rozproszone uzwojenie SynRM wykazało nieco lepszą zdolność przeciążania, proponowane skoncentrowane uzwojenie SynRM będzie łatwiejsze do zbudowania ze względu na mniejszą liczbę szczelin stojana.* (***Modelowanie i analiza skoncentrowanych i rozproszonych synchronicznych silników reluktancyjnych o zmiennych fazach bezpośrednich***)

Keywords: Direct-Phase-Variable Model, Finite Element Analysis, Synchronous reluctance motor, Winding Function Theory.
Słowa kluczowe: silnik reluktancyjny, silnik synchronicz\ny, metoda elementów skończonych.

Introduction

The Synchronous reluctance motor (SynRM) is singly salient and the rotor (without field-excitation windings) is constructed in a way that uses the principle of reluctance to produce electromechanical energy conversion [1].
Recently, the SynRM is considered an attractive alternative to the induction motor (IM) for constant speed applications. The experimental comparisons show that the SynRM with a transversely laminated rotor can provide 10 – 20% more torque than the IM [2,3]. A rotor cage is needed for good damping if the SynRM is line-start. The advantages of the SynRM are the simple rugged structure, low cost in manufacturing, short-time overload capability, no excitation losses on the rotor, high-speed capability, easy field weakening capability etc. [4,5]. Some shortcomings of the SynRM are poor power factor, poor torque performance, and low output power. Reasonable successes have been achieved in improving these shortcomings by optimizing different rotor structures with flux barriers to improving saliency [6–8], the use of permanent magnets to improve saliency [9, 10], and the use of dual-windings with capacitance injection to improve power factor [11, 12].

A comprehensive procedure for calculation of machine inductances of the conventional distributed SynRM was presented in [13], and calculation of inductances and torque of an axially laminated SynRM was presented in [14]. Direct-phase-variable modelling of a conventional distributed SynRM considering spatial harmonics was presented in [15], and the performance of the machines was observed though not validated by FEA. Similar procedures used in [15] were employed in this study. The consideration of harmonics was necessary because concentrated windings produce a significant amount of MMF harmonics [16], however appropriate slot and pole combinations have the capability of achieving sinusoidal MMF waveforms, and MMF harmonics cause flux variation in the machine airgap and this result in induced rotor losses. A five-phase direct phase variable (DPV) model of the SynRM and the permanent magnet synchronous motor was presented in [17, 18], results showed that the DPV and the Finite Element Analysis (FEA) model were in good agreement.

The purpose of this paper was to model and analyze a proposed concentrated (overlapping) and conventional distributed winding SynRM in direct-phase variables compare their performance characteristics, and validate results gotten with that of FEA to show the feasibility, accuracy and existence of harmonics in the models.

Determination of Machine Inductances

The machine models considered in this study were a proposed (a) 12-slot full-pitch single layer concentrated winding and (b) 36-slot full-pitch single layer distributed winding, with dimensions presented in Table 1. The winding clock diagrams are shown in Fig. 1. The traditional dumbbell rotor with damper windings was used for this study.

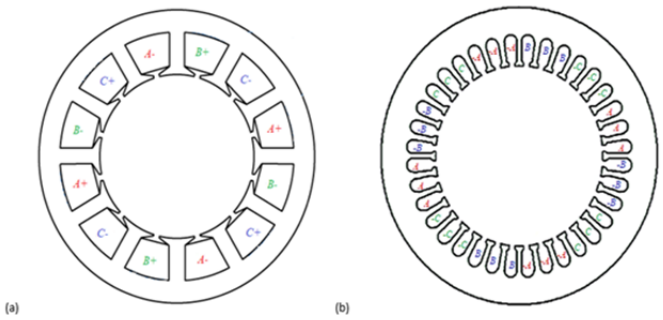

Fig. 1. Winding clock diagrams of (a) concentrated winding SynRM (b) distributed winding SynRM

The determination of machine inductances is crucial as it defines the behaviour of the SynRM since it influences the reluctance torque of the SynRM. The expression for the calculation of stator self and mutual inductances is presented in equations (1) and (2)

(1) $L_{AA} = \mu_0 rl \int_0^{2\pi} N_A^2(\phi) g^{-1}(\phi, \theta_r) d\phi$

(2) $L_{AB} = \mu_0 rl \int_0^{2\pi} n_A(\phi) N_B(\phi) g^{-1}(\phi, \theta_r) d\phi$

where μ_0 is the magnetic permeability, r is the machine radius, l is the stack length.

The winding function (expression) of an arbitrary phase A, with Pp number of pole-pairs by Fourier series, can be written as (3), [15]

(3) $N_K(\phi) = \sum_{n=1,3,5,\ldots}^{\infty} \frac{4N_t k_{wn}}{P_p n\pi} \cos P_p n(\varphi - \kappa \frac{2\pi}{mP_p})$

k = 0, 1,2, for phases A, B, C, respectively, showing the phase shift of the various phases, N_t is the number of turns per pole per phase, P_p is the number of pole pairs, n is the harmonic order, m is the number of phases, φ is the stator circumferential position and k_{wn} is the winding factor for the nth harmonic.

Table 1. Machine dimensions

Machine dimensions	Values	
Stator outer radius	105.2mm	
Stator inner radius	67.99mm	
Rotor radius	67.69mm	
Effective stack length	160.22	
Airgap length at pole face, g_1	0.4mm	
Airgap length between poles, g_2	21.3mm	
Stator slot depth	18mm	
Ratio of pole arc to pole pitch	2/3	
Number of Pole pairs	2	
Winding connection	Y	
Number of winding layers	1	
	Distributed winding	Concentrated winding
Number of slots	36	12
Number of turns	32	96
Stator slot pitch	10°	30°

The airgap expression is presented in (4), [14]

(4) $g(\phi, \theta_r) = k_c g_1 + \beta k_c (g_2 - g_1) + \frac{2}{\pi} \sum_{n=1}^{\infty} \frac{1}{n} k_c (g_2 - g_1) \times \sin n\beta\pi \cos 2P_p n(\phi - \theta_r)$

where g_1 and g_2 are the airgaps at pole face and between poles, β is the pole arc to pole pitch ratio, k_c is the Carter coefficient, accounting for slot openings, θ_r is the angular position of the rotor and ϕ is the stator circumferential position.

The stator to rotor mutual inductances was determined using (2), but the rotor cage winding expression in the rotor reference frame was employed. The actual rotor winding expression is presented in equations (5) and (6) [19]

(5) $N_{dr}(\phi) = \frac{4}{\pi} \sin^2\left(\frac{\gamma}{2}\right) + \frac{4}{\pi} \sin^2\left(\frac{3\gamma}{2}\right) + \frac{4}{\pi} \sin^2\left(\frac{5\gamma}{2}\right)$

(6) $N_{qr}(\phi) = \frac{4}{\pi}\left[\cos\frac{\gamma}{2} - \cos\frac{3\gamma}{2}\right]^2 + \frac{4}{\pi}\left[\cos\frac{3\gamma}{2} - \cos\frac{5\gamma}{2}\right]^2$

The fundamental (d-q) components of the d-axis and q-axis rotor winding expression derived from [20], is shown in equations (7) and (8)

(7) $N_{dr}(\varphi, \theta_r) = \frac{2}{\pi}\left[n_m + 2\sin^2\frac{\gamma}{2} - \frac{\sin(n_m\gamma)\cos(n_p\gamma)}{\sin\gamma}\right] \sin\xi$

(8) $N_{qr}(\varphi, \theta_r) = \frac{8}{\pi}\left[n_m - \frac{\cos\left(\gamma\frac{n_b - 1}{2}\right)\sin(n_m\gamma)}{\sin\gamma}\right] \sin^2\frac{\gamma}{2}\cos\xi$

where $n_m = 1/2(n_b - 2)$, $n_p = 1/2(n_b + 2)$, n_b is the number of rotor bars per pole, γ is an angle known as the rotor slot span and $\xi = (\varphi - \theta_r)$.

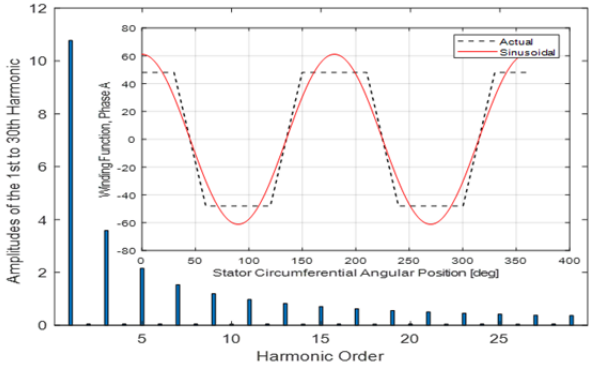

Fig. 2. Phase A winding function of a 12-slot concentrated stator winding showing the actual, the sinusoidal and the harmonic spectrum (Sum up to the 30th harmonic)

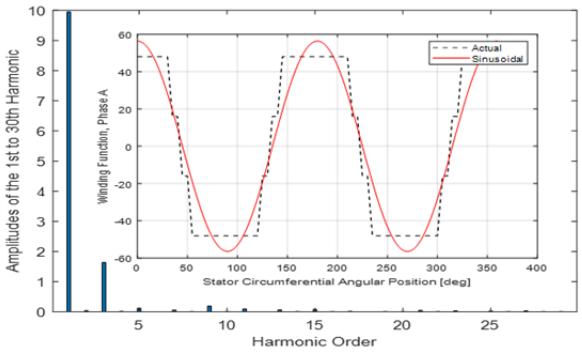

Fig. 3. Phase A winding function of a 36-slot distributed stator winding showing the actual, the sinusoidal and the harmonic spectrum (Sum up to the 30th harmonic)

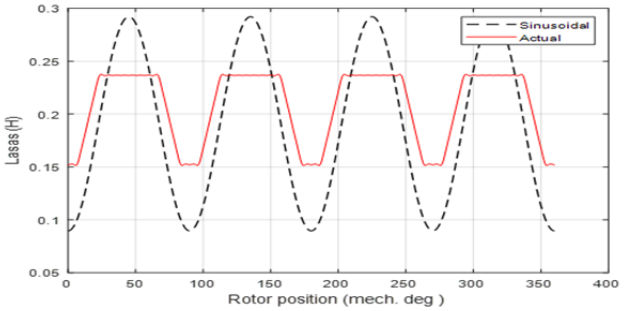

Fig. 4. Self-inductance of concentrated stator windings, for phase A, Lasas

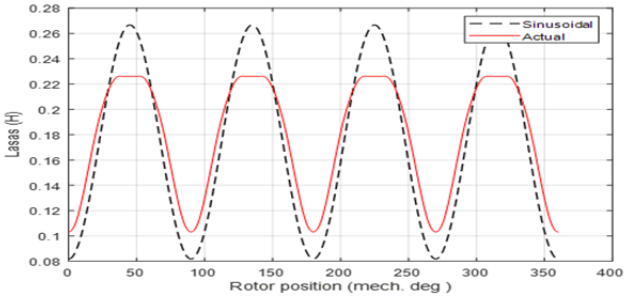

Fig. 5. Self-inductance of distributed stator windings, for phase A, Lasas

The phase A actual (including MMF harmonics) and sinusoidal winding function of the concentrated and

distributed winding configurations, their harmonic spectra are shown in Fig. 2 and Fig. 3. The concentrated winding configuration is seen to have more MMF harmonics than the distributed winding. The self-inductances are presented in Fig. 4 and 5, while the stator to rotor mutual-inductances are shown in Fig. 6 and Fig. 7, calculated using equation (1) and (2).

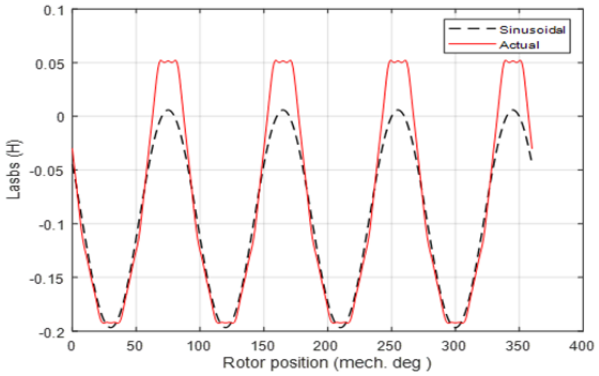

Fig. 6. Mutual-inductance between concentrated stator winding, of phase A and phase B, Lasbs

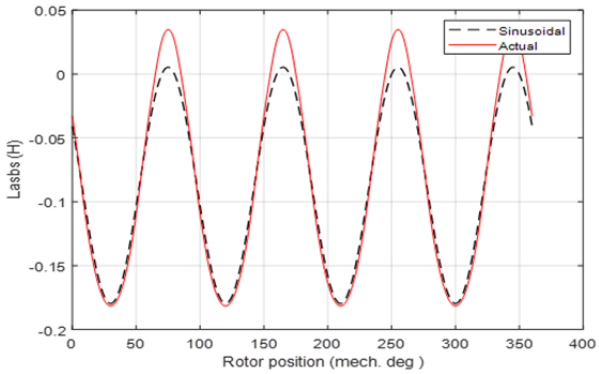

Fig. 7. Mutual-inductance between distributed stator winding, for phase A and phase B, Lasbs

Machine Equations

The voltage equations for a conventional three-phase line-start SynRM is given in (9) and can be written in matrix form as seen in (10)

(9) $V = IR + \frac{d}{dt}(LI)$

(10) $$\begin{bmatrix} V_{as} \\ V_{bs} \\ V_{cs} \\ V_{qr} \\ V_{dr} \end{bmatrix} = \begin{bmatrix} r_{as} & 0 & 0 & 0 & 0 \\ 0 & r_{bs} & 0 & 0 & 0 \\ 0 & 0 & r_{cs} & 0 & 0 \\ 0 & 0 & 0 & r_{qr} & 0 \\ 0 & 0 & 0 & 0 & r_{dr} \end{bmatrix} \begin{bmatrix} i_{as} \\ i_{bs} \\ i_{cs} \\ i_{qr} \\ i_{dr} \end{bmatrix} + \frac{d}{dt}\left(\begin{bmatrix} L_{asas} & L_{asbs} & L_{ascs} & L_{asqr} & L_{asdr} \\ L_{bsas} & L_{bsbs} & L_{bscs} & L_{bsqr} & L_{bsdr} \\ L_{csas} & L_{csbs} & L_{cscs} & L_{csqr} & L_{csdr} \\ L_{qras} & L_{qrbs} & L_{qrcs} & L_{qrqr} & L_{qrdr} \\ L_{dras} & L_{drbs} & L_{drcs} & L_{drqr} & L_{drdr} \end{bmatrix} \begin{bmatrix} i_{as} \\ i_{bs} \\ i_{cs} \\ i_{qr} \\ i_{dr} \end{bmatrix} \right)$$

Equation (9) can be re-arranged to achieve equation (11)

(11) $\frac{dI}{dt} = \left[V - I\left(R + \omega_r \times \frac{dL(\theta_r)}{d\theta_r}\right)\right] \times \left(L(\theta_r)\right)^{-1}$

where, $\omega_r = \frac{d(\theta_r)}{dt}$, and θ_r is the angular position of the rotor.

The stator self and mutual inductances in the voltage (10) can be expressed as (12) and (13)

(12) $L_{asas} = L_{ls} + L_1 - L_2 \cos 2\theta_r$

(13) $L_{asbs} = -\frac{1}{2}L_1 - L_2 \cos 2\left(\theta_r - \frac{\pi}{3}\right)$

where,

(14) $L_1 = \frac{1}{3}\left(L_{md} + L_{mq}\right)$

(15) $L_2 = \frac{1}{3}\left(L_{md} - L_{mq}\right)$

where L_{md} and L_{mq} are the magnetizing d- and q-axis inductances. L_{ls} is the stator leakage inductance. The self and mutual stator inductances for the other phases are similar to the equations (12) and (13) with a phase shift of 2π/3.

The stator to rotor mutual inductance was given in equations (16) and (17)

(16) $L_{asqr} = L_{mq} \cos(\theta_r)$

(17) $L_{asdr} = L_{md} \sin(\theta_r)$

The stator to rotor mutual inductances involving other phases of the motor is similar to the equations (16) and (17) with a phase shift of 2π/3.

The electromagnetic torque equation of the SynRM was expressed in equation (18)

(18) $T_e = \frac{P}{2}\left\{\frac{1}{2}[I_S]^T \frac{\partial[L_{SS}(\theta_r)]}{\partial\theta_r}[I_S] + [I_S]^T \frac{\partial[L_{SR}(\theta_r)]}{\partial\theta_r}[I_R]\right\}$

where,

(19) $[I_S] = [i_{as} \quad i_{bs} \quad i_{cs}]^T$

(20) $[I_R] = [i_{qr} \quad i_{dr}]^T$

I_s and I_r are the stator and rotor current respectively. The submatrices $[L_{ss}(\theta_r)]$ and $[L_{sr}(\theta_r)]$ are the stator and stator-rotor inductances in equation (10).

The relationship between the electromagnetic torque of the machine T_e and rotor speed ω_r is given in the mechanical dynamic equation (19) while ignoring the effect of friction.

(21) $T_e = J\left(\frac{2}{P}\right)p_p\omega_r + T_L$

Dynamic Simulation of the Line-Start Synchronous Reluctance Motors Using MATLAB/Simulink

The dynamic simulation of the concentrated and distributed winding SynRM was carried out in direct-phase variables in the MATLAB/Simulink environment. It should be noted that the direct-phase model that considers only the fundamental MMF yields almost the same result as the d-q model. Also, note that a line-start three-phase supply consists of only the fundamental and the reason is that triplen harmonics are co-phasal and are eliminated from the line-to-line waveforms.

The SynRM has a constant supply voltage of 370V at a frequency of 50Hz. The machine parameters were extrapolated from [15] and the machine dimensions presented in Table 1. were used for the simulation. The stator winding resistances R_{sc} = 1.35Ω and R_{sd} = 1.504Ω for the concentrated and distributed winding respectively. The rotor d – and q – axis inductances and resistances were: L_{lqr} = 6.2mH, L_{ldr} = 5.5mH, R_{qr} = 0.25Ω and R_{dr} = 0.12Ω.

The simulation time of 6 seconds was used and a load torque of 25 N-m (70% of rated torque) was introduced after 3 seconds. The rated torque of the machines was calculated to be 35 Nm. The performance characteristics of the machine were then observed. The performance characteristics of the line-start concentrated and distributed winding SynRM considering just the fundamental, simulated in MATLAB/Simulink were presented in Fig. 8 – Fig. 15. The simulation of the same machine models was also carried in in ANSYS Electronics Desktop which takes into consideration all harmonics is presented in the next section.

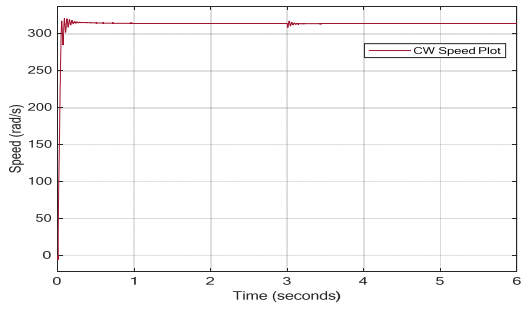

Fig. 8. Concentrated winding SynRM speed against time

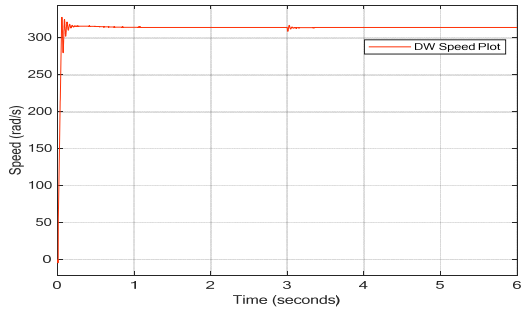

Fig. 9. Distributed winding SynRM speed against time

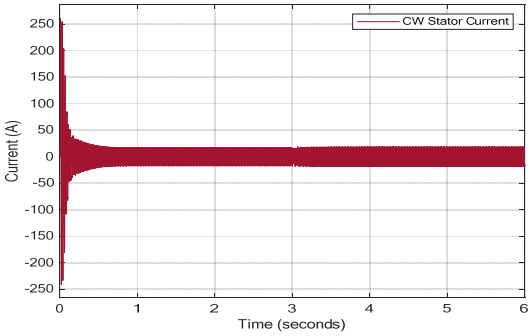

Fig. 10. Concentrated winding SynRM phase A current against time with the inclusion of winding harmonics

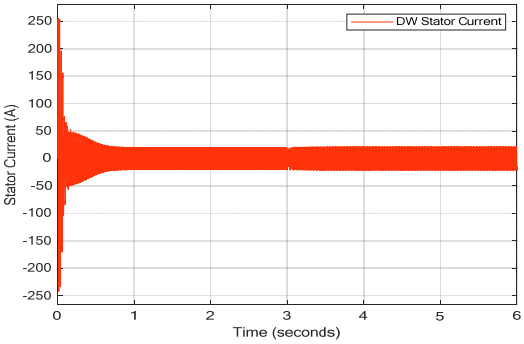

Fig. 11. Distributed winding SynRM phase A current against time

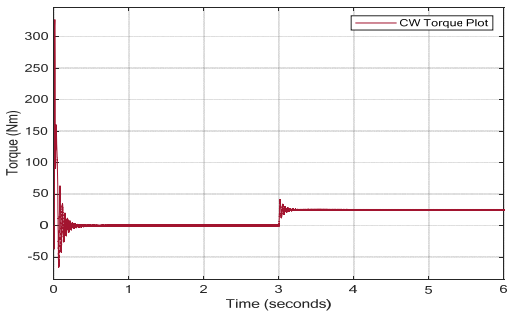

Fig. 12. Concentrated winding Torque against time

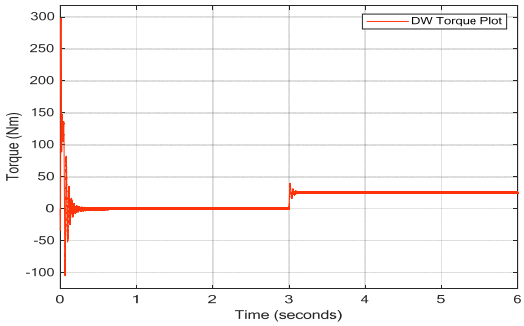

Fig. 13. Distributed winding SynRM Torque against time

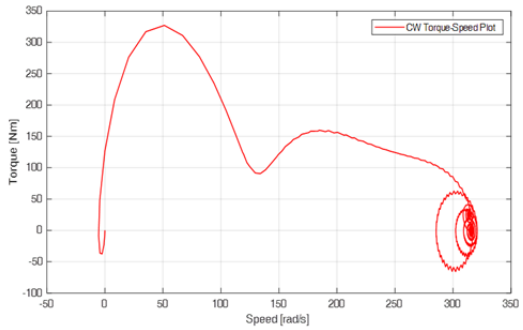

Fig. 14. Concentrated winding Torque against Speed

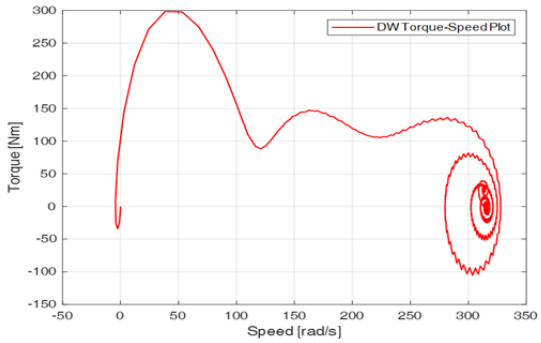

Fig. 15. Distributed winding Torque against Speed

Dynamic Simulation Using Finite Element Analysis

Ansys Maxwell Electronics Desktop Finite Element Analysis software was used for the analysis of the machine models, using the design parameters given in Table 1 for validation of the models. The SynRMs were also simulated as Line-start with a supply voltage of 370V at a frequency of 50Hz. The simulation time of 2 seconds was used and a load torque of 25Nm was introduced after 1 second. The Speed, Phase A currents, and Torque performance characteristics of the machine were then observed in Fig. 20. – Fig. 25.

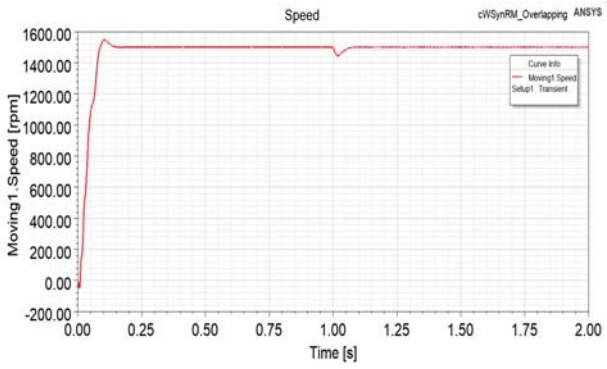

Fig. 20. Concentrated winding SynRM FEA Speed characteristic

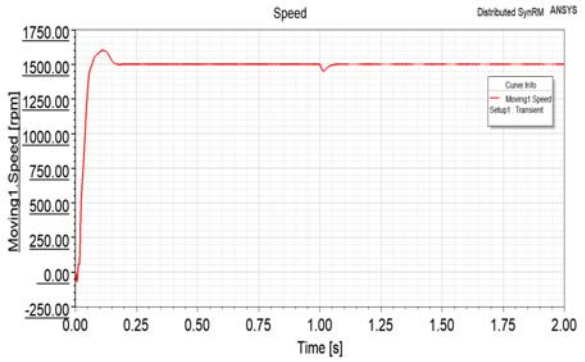

Fig. 21. Distributed winding SynRM FEA Speed characteristic

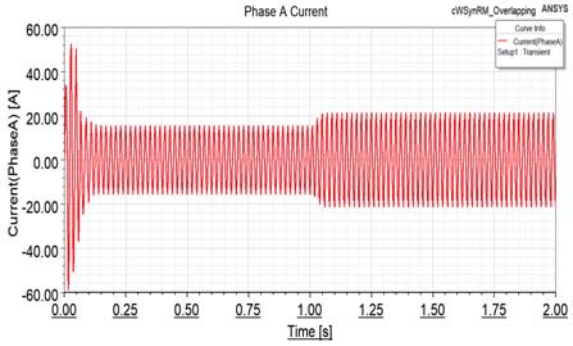

Fig. 22. Concentrated winding SynRM FEA phase A stator current

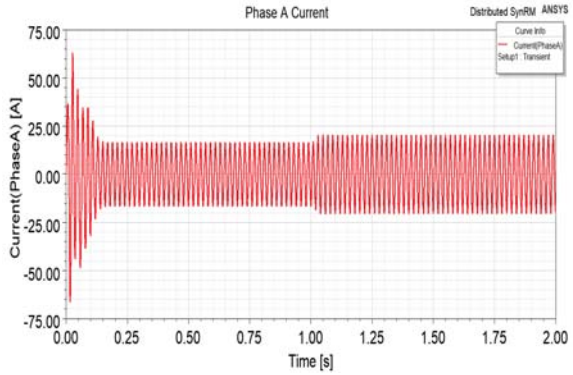

Fig. 23. Distributed winding SynRM FEA phase A stator current

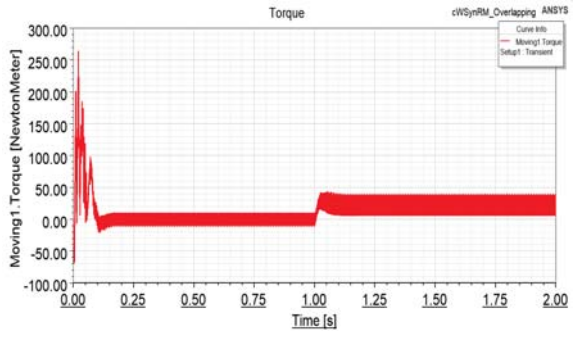

Fig. 24. Concentrated winding SynRM FEA Torque characteristic

The torque plots of the direct-phase variable models presented in Fig. 12 and Fig. 13 did not show the evidence of torque ripples caused by MMF harmonics and airgap permeance harmonics, while the FEA torque plots in Fig. 24 and Fig. 26 showed the presence of such harmonics which resulted in torque ripples.

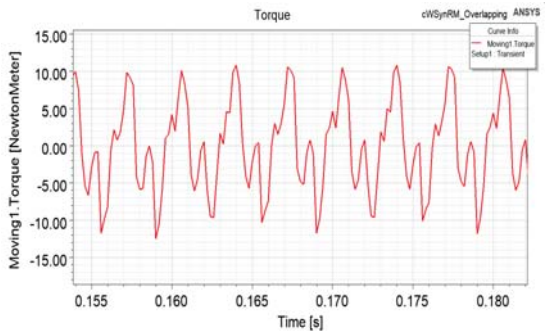

Fig. 25. Concentrated winding SynRM FEA Torque characteristic showing the Torque ripples

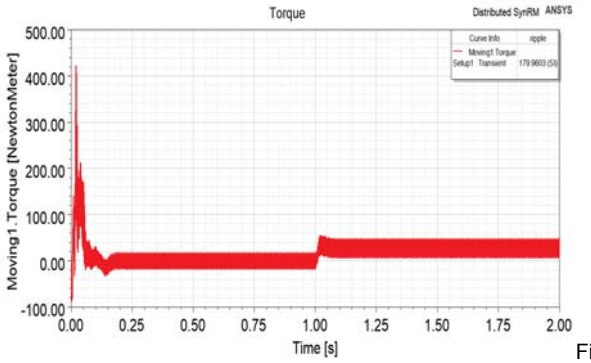

Fig. 26. Distributed winding SynRM FEA Torque characteristic

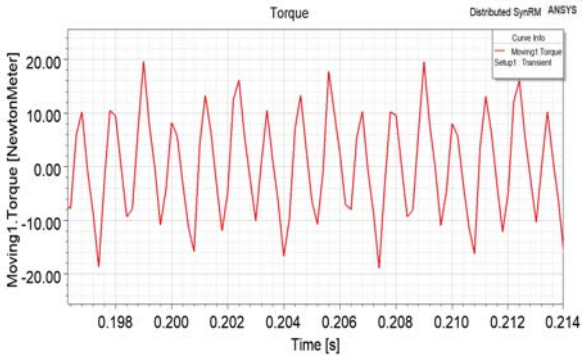

Fig. 27. Distributed winding SynRM FEA Torque characteristic showing the Torque ripples

The torque ripple plots of Fig. 25 and Fig. 27 were extrapolated from the torque performance plots of Fig. 24 and Fig. 26 for both FEA machine models. The extrapolation was done before the introduction of load torque. From the torque ripple plot of the concentrated winding SynRM (Fig. 25), a maximum ripple value of 10.62Nm and a minimum ripple value of -11.85Nm was observed. The torque ripple plot of the distributed winding SynRM (Fig. 27) showed a maximum ripple value of 19.23Nm and a minimum ripple value of -19.07Nm.

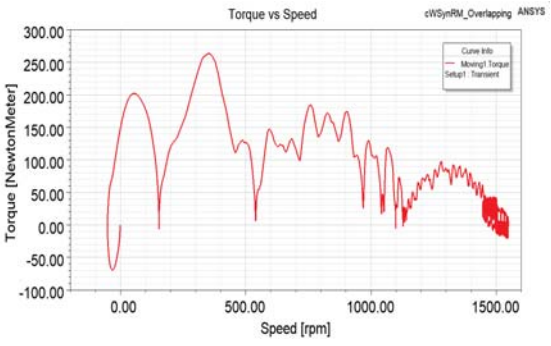

Fig. 28. Concentrated winding SynRM FEA Torque-Speed characteristic

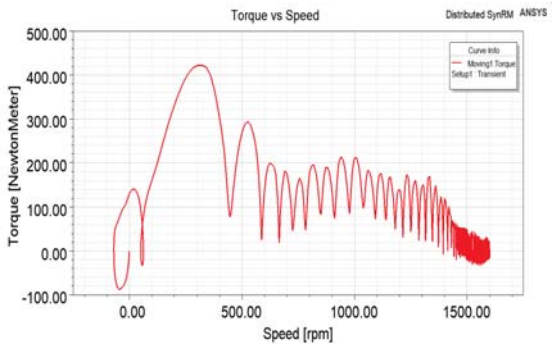

Fig. 29. Distributed winding SynRM FEA Torque-Speed characteristic

The loading capabilities of the concentrated and distributed winding SynRM were determined by the monitoring of the speed characteristics of both the concentrated and distributed winding SynRM. The machines were placed on Ramp load in ANSYS and a load torque of 2 Nm starting value was introduced from zero seconds. The machines were simulated for 4 seconds and it was observed that the maximum load torque of the concentrated winding SynRM was 31.69 Nm at 3.06 seconds as presented in Fig. 28. The maximum load torque of the distributed winding SynRM was 38.38 Nm at 3.73 seconds as seen in Fig. 29.

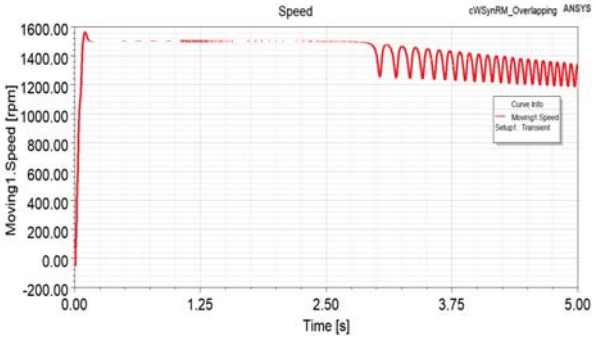

Fig. 30. Concentrated winding SynRM FEA Speed characteristic under Ramp loading

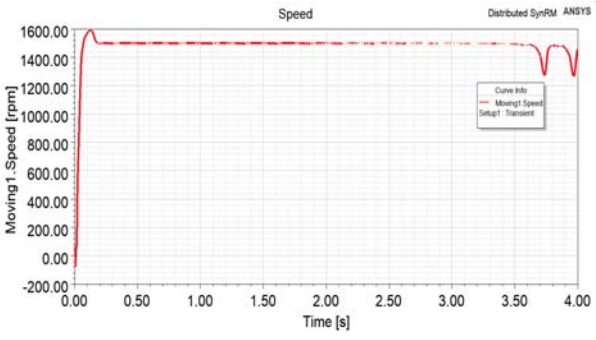

Fig. 31. Distributed winding SynRM FEA Speed characteristic under Ramp loading

Conclusion

The concentrated and distributed winding synchronous reluctance motors were simulated using a combination of winding function theory and the direct-phase variable model. The motors were simulated as Line-start in direct-phase variables. Actual (sums to the 30th harmonic) and sinusoidal inductance calculations of the various winding topographies using MATLAB/Simulink showed the presence of winding harmonics. It was observed that results from the direct-phase variable (DPV) models for the Line-start SynRMs were similar to the results from the Finite Element Analysis (FEA) Line-start simulation which included all spatial harmonics, as seen in the torque plots. Thus, FEA models which included all harmonics were more precise nonetheless it does not annul results gotten from the direct-phase variable models which utilized just the fundamental MMF. The results from both methods compare favourably. This also implies that the direct-phase variable model can be applied to other AC machines since it gives some form and accuracy and is faster in simulation time when compared to FEA.

The study also showed that the distributed winding SynRM had a better overload capability when compared to its concentrated winding counterpart. The simulation showed that distributed winding SynRM could tolerate torque overload of a 9.66% increase, while the concentrated winding SynRM showed a decrease of 9.46% when compared to the rated torque.

Although the distributed winding SynRM gave better torque overload capability than the proposed concentrated winding SynRM with a higher number of turns, the concentrated winding SynRM will be easier to construct as it has fewer slots. The key benefits of adopting the concentrated winding topology, such as reduced axial length, compact design, shorter coil-ends which results in lower copper losses and higher efficiency can be utilized.

***Authors**: Engr. Ayebatonye Epemu, Department of Electrical/Electronic Engineering, Federal University of Petroleum Resources, Effurun, Delta State, Nigeria, E-mail: epemu.ayebatonye@fupre.edu.ng; Dr Pauline Obe (Corresponding Author), Department of Industrial Technical Education, University of Nigeria, Nsukka, Enugu State, Nigeria, E-mail: pauline.obe@unn.edu.ng; Engr. Prof. Emeka Obe Department of Electrical Engineering, University of Nigeria, Nsukka, Enugu State, Nigeria, E-mail: simon.obe@unn.edu.ng*

REFERENCES

[1] Kostko, J., “Polyphase reaction synchronous motors,” J. Am. Inst. Electr. Eng., 42(1923), no. 11,1162–1168
[2] Boglietti, A., Cavagnino, A., Pastorelli, M., and Vagati, A., “Experimental Comparison of Induction and Synchronous Reluctance Motors Performance,” in IEEE Industry Applications Conference, (2005), 474–479
[3] Spargo, C., “Synchronous Reluctance Technology-Part I,” Durham Res. Online, 44(2016), no. 1,1–5
[4] Lipo, T., “Novel Reluctance Machine Concepts for Variable Speed Drive,” in 6th Mediterranean Electrotechnical Conference Proceedings, (1991), 34–43
[5] Vagati, A., “The synchronous reluctance solution: A new alternative in AC drives,” IEEE IECON conference, 1(1994), 1–13
[6] Martis, C., “New Shape of Rotor Flux Barriers in Synchronous Reluctance Machines Based on Zhukovski Curves,” in IEEE International Symposium on advanced topics in electrical engineering, (2015), 221–224
[7] Ma, X., Li, G., Zhu, Z., Jewell, G., and Green, J., “Investigation on Synchronous Reluctance Machines with Different Rotor Topologies and Winding Configurations,” IET Electr. Power Appl., (2017)1–17
[8] Hu, Y., Chen, B., Xiao, Y., Shi, J., and Li, L., “Study on the Influence of Design and Optimization of Rotor Bars on Parameters of a Line-Start Synchronous Reluctance Motor,” IEEE Trans. Ind. Appl., 56(2020) no. 2, 1368–1376
[9] Zhao, W., Lipo, T., and Kwon, B., “Performance Improvement of Ferrite-Assisted Synchronous Reluctance Machines Using Asymmetrical Rotor Configuration.,” IEEE Trans. Magn., 51(2015), no.11,1-1
[10] Siadatan, A., Goltieb, J., and Afjei, E., “Comparison of power factor between permanent magnet assisted synchronous reluctance motor with neodymium-iron-boron and ferrite

magnets," Int. Symp. Power Electron. Electr. Drives, Autom. Motion, (2020), 144–150
[11] Ogunjuyigbe, A., Jimoh, A., Nicolae, D., and Obe, E., "Analysis of synchronous reluctance machine with magnetically coupled three-phase windings and reactive power compensation," IET Electr. Power Appl., 4(2010), no. 4, 291–303
[12] Park, J., Bianchini, C., Bellini, A., Davoli, M., and Bianchi, N., "Experiment-based performance analysis for dual three-phase synchronous reluctance motor according to different winding configurations," Int. Symp. Power Electron. Electr. Drives, Autom. Motion, (2020), 478–483
[13] Obe, E., "Direct computation of ac machine inductances based on winding function theory," Energy Convers. Manag., 50(2009), no. 3, 539–542
[14] Obe, E., "Calculation of inductances and torque of an axially laminated synchronous reluctance motor," IET Electr. Power Appl., 4(2010), 783–792
[15] Obe, E., and Binder, A., "Direct-phase-variable model of a synchronous reluctance motor including all slot and winding harmonics," Energy Convers. Manag., 52(2011), 284–291
[16] Cros, J., and Viarouge, P., "Synthesis of High-Performance PM Motors With Concentrated Windings," IEEE Energy Convers., 17(2002), no. 2, 248–253
[17] Umoh, G., Ogbuka, C., and Obe, E., "Modelling and analysis of five-phase permanent magnet synchronous motor in machine variables," Prz. Elektrotechniczny, 96(2020), no. 1, pp. 87–92, 2020
[18] Umoh, G., Obe, C., Ogbuka, C., Ekpo, G., and Obe, E., "Direct-phase variable modelling and analysis of five-phase synchronous reluctance motor for direct-on-line starting," Prz. Elektrotechniczny, 97(2020), no. 1, 24–29
[19] Lipo, T., Introduction to AC Machine Design, First Edition, New Jersey: Wiley, 2017
[20] Lipo, T., Analysis of Synchronous Machines, Second Edition. New York: Taylor & Francis Group, LLC, 2012